H1prelim 08-074 Submitted to

34th Int. Conf. on High Energy Physics, ICHEP2008, July 30-August 4, 2008, Philadelphia
Abstract: **860**
Parallel Session **QCD/Lattice**

Electronic Access: www-h1.desy.de/h1/www/publications/conf/conf_list.html

$D^{*\pm}$-Meson Production at Large Q^2 in Deep Inelastic Electron-Proton Scattering at HERA

H1 Collaboration

Abstract

Inclusive production of $D^{*\pm}$-mesons in deep inelastic scattering at HERA is studied at high photon virtualities $Q^2 > 100$ GeV^2 for the first time with the H1 experiment. The data were collected during the years 2004-2007 and correspond to an integrated luminosity of 351 pb^{-1}. D^*-mesons are reconstructed in their decays $D^{*\pm} \rightarrow D^0 + \pi^{\pm}_{slow} \rightarrow K^{\mp} + \pi^{\pm} + \pi^{\pm}_{slow}$. The visible range for the measurement covers the pseudorapidity interval $|\eta(D^*)|$ <1.5, transverse momenta $p_t(D^*)$>1.5 GeV, and inelasticity in the scattering process $0.02 < y < 0.7$. Differential cross sections are compared to predictions from the next-to-leading order calculation HVQDIS and the leading order Monte Carlo codes RAPGAP and CASCADE.

1 Introduction

The description of open heavy flavour production in electron[1] proton collisions is based on perturbative QCD. In leading order (LO), the photon gluon fusion process ($\gamma g \to Q\overline{Q}$), depicted in Fig. 1 is the dominant contribution, i.e. the virtual photon couples to the gluon in the proton through a heavy quark-antiquark pair. The boson-gluon fusion process itself is interesting because it may constrain the gluon density in the proton as demonstrated in previous analyses at lower photon virtuality Q^2 [1].

This paper presents the first analysis of $D^{*\pm}$-meson production for large $Q^2 > 100$ GeV^2 with the H1 detector at HERA at a centre-of-mass energy of 320 GeV. Charm events are tagged via full reconstruction of $D^{*\pm}$-mesons using the decay chain $D^{*\pm} \to D^0 + \pi^{\pm}_{slow} \to K^{\mp} + \pi^{\pm} + \pi^{\pm}_{slow}$.

2 Theoretical models

The leading order treatment of heavy flavour production has been extended to next-to-leading order (NLO) for which calculations in several schemes are available [2–6]. All approaches assume the scale to be hard enough to apply pQCD and to guarantee the validity of the factorisation theorem. Here, the *massive approach* is adopted, i.e. a fixed order calculation with massive quarks assuming three active flavours in the proton. The momentum densities of the three light quarks and the gluon in the proton are evolved by the DGLAP equations [7]. The heavy quarks are assumed to be produced only at the perturbative level [2] via photon gluon fusion. Based on the NLO calculations of order α_s^2 in the coefficient functions [2] programs for different applications were developed in the fixed-flavour-number-scheme (FFNS). The Riemersma program [3] allows the calculation of inclusive quantities of heavy quark production, like $F_2^c(x, Q^2)$, while the HVQDIS program [4] allows the calculation of exclusive quantities by providing the four-momenta of the outgoing partons.

Inclusive charmed meson production cross sections are calculated using the HVQDIS program after fragmenting the charm quarks in the photon - proton centre-of-mass frame into $D^{*\pm}$ mesons. The Kartvelishvili *et al.* fragmentation function [8] is used, which is controlled by a single parameter α. The charm fragmentation function was measured at H1 using inclusive $D^{*\pm}$ meson production associated with jet production. Differences in the measured non-pertubative fragmentation function close to and well above threshold of charm production has been reported [9]. To account for the experimental observation a $\hat{s}$-dependent charm fragmentation function is introduced with $\alpha = 6.0$ for $\hat{s} < 70$ GeV^2 and $\alpha = 3.3$ otherwise. With this procedure it becomes possible to calculate differential inclusive $D^{*\pm}$ meson cross sections in the experimentally visible phase space region. To estimate the theoretical systematic uncertainty of the predictions for the kinematical regime of this paper the charm mass is varied between 1.3 GeV and 1.6 GeV, the factorization and renormalization scales are varied simultaneously around $0.5\mu < \mu < 2\mu$, with $\mu^2 = Q^2 + 4m_c^2$, and the fragmentation parameter is varied in the interval $2.9 < \alpha < 3.7$.

[1] Here and further electron denotes electron or positron

In addition the RAPGAP [10] and CASCADE [11, 12] Monte-Carlo simulations are used for comparison to the data. Both simulations are based on leading order matrix elements with the higher order corrections implemented via parton showers. Parton evolution according to the DGLAP [7] equations is used in the RAPGAP program. All events generated are passed through the full GEANT [13] based simulation of the H1 apparatus and are reconstructed using the same program chain as for the data. The RAPGAP based simulation has been used also to correct the data for the limited acceptance and efficiency of the detector.

CASCADE implies the intrinsic k_t factorisation and parton evolution according to the CCFM equations [14]. The latter is expected to be more appropriate to describe the parton evolution at small x, where the collinear assumption of a large longitudinal momentum compared to the transverse momentum of the partons might not be valid. In the parton cascade, gluons are emitted in an angular ordered manner to account for coherence effects. Due to this angular ordering, the gluon distribution depends on the maximum allowed angle in addition to the momentum fraction x and the transverse momentum of the propagator gluon. The cross section is then calculated according to the k_t-factorisation theorem by convoluting the unintegrated gluon density with the off-shell photon gluon fusion matrix element with massive quarks for the hard scattering process. The parametrisation set A0 [15] is used for the unintegrated gluon distribution of the proton.

3 Experimental method

3.1 H1 detector

A detailed description of the H1 detector can be found in [16]. In the following only detector components relevant to this analysis are briefly discussed. The origin of the H1 coordinate system is the nominal ep interaction point, with the direction of the proton beam defining the positive z-axis (forward direction). Transverse momenta are measured in the $x - y$ plane. Polar (Θ) and azimuthal (ϕ) angles are measured with respect to this reference system. The pseudorapidity is defined to be $\eta = -\ln\tan(\Theta/2)$. In the central region ($20^\circ < \Theta < 165^\circ$) the interaction region is surrounded by the central tracking system, which consists of a silicon vertex detector, drift chambers and multi-wire proportional chambers, all operated within a solenoidal magnetic field of 1.16 T. The trajectories of charged particles are measured in the central tracker with a transverse momentum resolution of $\sigma(p_t)/p_t \approx 0.005 p_t/\mathrm{GeV} \oplus 0.015$. In each event the ep interaction vertex is reconstructed from the measured charged tracks.

The liquid argon (LAr) sampling calorimeter [17] surrounds the tracking chambers. It has a polar angle coverage of $4^\circ < \Theta < 154^\circ$ and full azimuthal acceptance. It consists of an inner electromagnetic section with lead absorbers and an outer hadronic section with steel absorbers. Electromagnetic shower energies are measured with a precision of $\sigma(E)/E = 12\%\sqrt{E/\mathrm{GeV}} \oplus 1\%$ and hadronic energies with $\sigma(E)/E = 50\%\sqrt{E/\mathrm{GeV}} \oplus 2\%$, as determined in test beam experiments [18].

The luminosity is determined from the rate of the Bethe-Heitler process $ep \to ep\gamma$, measured using a photon detector located close to the beam pipe at $z = -103$ m, in the backward-direction.

At higher Q^2 DIS events are selected by requiring a scattered electron in the liquid argon calorimeter. For the electron in addition to the LAr cluster a matching track with the correct charge is required. The quantity z_{impact} describes the z-position where the extrapolation of the matched track subtends the area of beginning LAr. A cut on this quantity is normally applied to avoid the most backward edge of the LAr calorimeter where the electron reconstruction efficiency strongly decreases. The analysis presented here deals only with events triggered by the LAr calorimeter with a threshold of ~ 5 GeV (higher in forward region), for which the efficiency exceeds 97 %, determined by inspecting independent triggers.

3.2 Event selection and reconstruction of the kinematics

The full HERA-II statistics collected with H1 experiment in the years 2004-2007 is used for the analysis. This corresponds to the integrated luminosity of 351 pb^{-1}. The event selection and the acceptance of the H1 detector limits the cross section measurement to a visible range, whose boundaries are given in Tab. 1.

Photon virtuality (Q_e)	$100 < Q^2 < 1000$ GeV^2
Inelasticity ($y_{e\Sigma}$)	$0.02 < y < 0.7$
Pseudorapidity of D^*	$-1.5 < \eta(D^*) < 1.5$
Transverse momentum of D^* $^{a)}$	$p_t(D^*) > 1.5$ GeV

Table 1: Kinematical acceptance. ($^{a)}$ see text for details)

This analysis covers the DIS phase space $100 < Q^2 < 1000$ GeV^2 and $0.02 < y < 0.7$, where y quantifies the inelasticity of the interaction. These two variables as well as Bjorken-x are reconstructed from the four momenta of the scattered electron (E'_e, Θ_e), which is detected in the LAr-calorimeter excluding the most backward part ($z_{impact} > -1.9$ m), and the hadronic final state particles (y_h) using the electron-sigma method [20]: .

$$Q^2_e = E_e E'_e(1+\cos\Theta_e) \quad Q^2_\Sigma = \frac{E^2_e \cdot \sin^2\Theta_e}{1-y_\Sigma} \quad y_\Sigma = \frac{2y_h \cdot E'_e}{2y_h E'_e + E_e \cdot (1-\cos\Theta_e)} \tag{1}$$

$$y_h = \frac{\sum_i (E - p_{zi})}{2E_e} \qquad y_{e\Sigma} = \frac{Q^2_e}{x_\Sigma \cdot s} \qquad x_\Sigma = \frac{Q^2_\Sigma}{y_\Sigma \cdot s} \tag{2}$$

Events with charm quarks are identified via full reconstruction of the decay chain $D^{*\pm} \to D^0 + \pi^\pm_{slow} \to K^\mp + \pi^\pm + \pi^\pm_{slow}$. Due to the small difference between the masses of the D^* and D^0 mesons the pion π_s receives only small amount of kinetic energy and genuine $D^{*\pm}$-decays manifest themselves as a narrow peak in the distribution of the mass difference

$$\Delta m \equiv m(K\pi\pi_s) - m(K\pi), \tag{3}$$

as evident in Fig. 2. Unfortunately the branching ratio of this decay channel is only 2.35%, and the peak is superimposed on a background of primarily combinatorial origin.

The fraction $z(D^*)$ of the virtual photon momentum which is transfered to the D^* is calculated as

$$z(D^*) = \frac{E(D^*) - p_z(D^*)}{2yE_e} \tag{4}$$

The tracks of the decay particles are reconstructed in the central track detector, which determines the accepted D^* pseudorapidity range $\eta(D^*)$. The tracks have to fulfill quality criteria like minimal length and minimal number of hits in the central jet chambers, originate from the event vertex and have a transverse momentum exceeding either 0.5 GeV ($K^{\mp}, \pi^{\pm}$) or 70 MeV ($\pi^{\pm}_{slow}$). Furthermore the sum of the transverse momenta of $K^{\mp}$ and $\pi^{\pm}$ is required to be larger than 2 GeV, their invariant mass has to fall into the D^0 mass window $|m(K\pi) - m(D^0)| < 80$ MeV and the angle (Θ^*) of the kaon in the rest frame of the D^0 has to pass the cut $\cos\Theta^* > -0.7$. The lower limit of the transverse momentum of the D^* accepted in the analysis is slightly larger than that for the visible range and furthermore depends on Q^2 as

$$p_t(D^*)/\mathrm{GeV} > 3(\log(Q^2/\mathrm{GeV}^2) - 2) + 2 \tag{5}$$

The latter two conditions are imposed by background considerations described below.

To get an adequate description of the combinatorial background and for signal-to-background ratio (S/B) studies an additional wrong charge sample is selected by requiring a *doubly charged "D"* with otherwise the same cuts. This sample has no D^* signal but describes very well the background shape of the correct charge sample. The absolute normalisation differs only by a few percent (see Fig. 2). The combinatorial background is mainly reduced by the cuts on $p_t(D^*)$ and $\cos(\Theta^*)$ mentioned above.

The $p_t(D^*)$ spectrum of the signal and the background becomes harder with growing Q^2 since the complete hadronic final state receives a higher transversal boost. The cut applied in the analysis according eq. 5 takes this behavior into account. The function is motivated by signal-to-background ratio studies, which used a D^* Monte-Carlo simulation for the signal and the combinatorial background taken from the data. Further an acceptable extrapolation in $p_t(D^*)$ down to 1.5 GeV is required.

The cut on $\cos(\Theta^*)$ is motivated by the observation, that the corresponding distribution for the D^* signal is nearly flat, as expected for the isotropic decay topology, while the background strongly increases at low values of $\cos(\Theta^*)$. If the kaon candidate is emitted opposite to the D^0 flight direction, it has a lower momentum, which enhances the contamination from misidentified pions.

3.3 Signal extraction and determination of the cross section

Figure 2 shows Δm distribution for the complete data sample. The D^* signal at 145.5 MeV contains $N(D^*) = 497 \pm 37$ events above a background which matches closely the wrong charge sample. The fit to the mass-difference distribution for the full sample and in the individual bins assumes a symmetric Gauss-function for the signal and the Granet *et al.* parametrisation [21]

for the background. The latter accounts for the characteristic power law behavior of the phase space at threshold and includes an exponential damping term to describe the behavior at larger Δm:

$$f(m) = (m - m_\pi)^{p_1} \exp(-p_2 m - p_3 m^2) \tag{6}$$

A small tail of the signal to the higher mass side which has been observed in some higher statistics D^* analyses is not resolvable in this analysis and therefore not taken into account. The sum of the two functions is then fitted to the signal sample and simultaneously to the wrong charge sample. The shape of the background function for the two data samples is forced to be the same but the relative normalisation is left free. To keep the fit stable for the individual bins the width of the signal has been fixed to the value predicted by the simulation corrected for the small difference in resolution between data and Monte-Carlo observed for the full sample.

The total visible D^* production cross section or that in a certain bin is calculated as follows:

$$\sigma^{vis} = \frac{N(D^*)\,(1-R)}{\mathcal{L}\,\mathcal{B}(D^* \,\rightarrow\, K\pi\pi_s)\,\epsilon_{rec}\,(1-\delta_r)} \tag{7}$$

Here $N(D^*)$ is the number of D^* obtained from fit to the Δm - distribution, $\mathcal{L}$ the luminosity, $\mathcal{B}$ the branching ratio and ϵ_{rec} is the total reconstruction efficiency determined using the RAPGAP Monte Carlo[2]. For it the Monte-Carlo was reweighted in Q^2 to better describe the measured differential cross-sections.

By the D^0 mass window cut also small contributions from other deacay channels like

$$D^* \;\longrightarrow\; (KK, \pi\pi, \pi\pi\pi^0, Kl\nu_l)\,\pi_s \tag{8}$$

are accepted. The amount of these reflections is determined from Monte-Carlo to be $R = (4.4 \pm 0.5)\%$ nearly independent of the D^* transverse momentum. This contribution is subtracted in the cross sections according eq. 7.

Finally, to get to the visible cross sections at the Born level the reconstruction efficiency has to be corrected for initial and final state QED radiation. The corresponding correction δ_r, varying between 2 and 4 %, is evaluated comparing at the generator level Monte Carlo data with and without radiative corrections using the HERACLES-code [23] interfaced to the RAPGAP Monte Carlo for the corresponding kinematics bin.

3.4 Systematic errors

The following sources of systematic errors have been considered:

- The single track finding efficiency has been determined up to an uncertainty of 2%, translating to 6% per D^*.

[2]The trigger efficiency is determined without Monte-Carlo simulation by inspecting independent triggers

- The vertex fit efficiency has been systematically studied for D^* analysis at medium Q^2 [24] and found to be subject to an uncertainty 2.5% per D^*.
- The systematic error associated to the signal extraction has been estimated by comparing the results from the fits to those obtained by statistical subtraction of the interpolated background and by varying the scale factor for the fixed Gausssian width within its uncertainty. It amounts to 5 % at most.
- The loss of signal events outside the accepted window around the D^0 mass differs between data and Monte Carlo due to resolution effects between 0.5 and 5 % (last Q^2) bin.
- The uncertainty stemming from possible photoproduction background is below 1 %.
- To estimate the systematic uncertainties from the models the acceptances for each bin are calculated both with the RAPGAP and the CASCADE Monte Carlo simulation. The considerable differences are taken as systematic error ranging from 0.5% to 17% (last x bin).
- The uncertainty of the energy of the scattered electron of 1.5% and of the hadronic final state energy of 2% may change the cross section for a given bin between 0.5% to 10% (last $z(D^*)$ bin) for the electron scale and from 0.5% to 4% for the hadronic scale. Similarly the uncertainty in the determination of the electron angle Θ_e of 3 mrad translates into a possible variation of the cross section between 0.5% and 1.5% (last Q^2 bin)
- The trigger efficiency is known with an uncertainty of 1%, the branching ratio for the decay channel used in this analysis with an uncertainty of 2.3%, and the luminosity with an uncertainty of 3.2%.

Adding these contributions in quadrature leads to systematic errors varying between 8 % and 21 %

4 Results and conclusions

This analysis yields for the total cross section in the visible range as given in Tab. 1

$$\sigma^{tot}_{vis}(e^{\pm}p \to e^{\pm}D^{*\pm}X) = 243 \pm 18\,(\text{stat.}) \pm 25\,(\text{syst.})\ \text{pb},$$

to be compared with the HVQDIS [4] prediction of

$$\sigma^{tot}_{vis}(e^{\pm}p \to e^{\pm}D^{*\pm}X) = 251\ {}^{+\,6}_{-\,7}\,(\text{model})\ \text{pb}.$$

The agreement is very good and apparently the model uncertainties have only minor influence on the prediction at large Q^2.

Figures 3 and 4 show the measured differential cross section either in bins of $\log Q^2$ and $\log x$, or in bins of $p_t(D^*)$, $\eta(D^*)$ and $z(D^*)$, respectively, compared to the Monte Carlo simulations RAPGAP [10] and CASCADE [11] as well as to the NLO calculation HVQDIS [4].

The latter describes all data distributions well, while RAPGAP and CASCADE fail to describe the Q^2 dependence, and CASCADE the $p_t(D^*)$-dependence as well.

The failure to describe the Q^2-dependence becomes more evident from Fig. 5, where the data from the present analysis are combined with those from an analysis at lower Q^2 [22, 24]. RAPGAP with the parton density CTEQ6$\ell\ell$ [25] describes the data at medium Q^2 well, while the more recent PDF-set CTEQ65m [26] gives a better description of the high Q^2 data, which explains why it was used for the determination of the acceptances here. Neither PDF-set accounts for the slope over the complete range, however. To a lesser degree this is also true for the CASCADE prediction. The best description of the data provides the NLO HVQDIS calculation using the PDF-set MRST2004FF3nlo [27].

Acknowledgements

We are grateful to the HERA machine group whose outstanding efforts have made this experiment possible. We thank the engineers and technicians for their work in constructing and maintaining the H1 detector, our funding agencies for financial support, the DESY technical staff for continual assistance and the DESY directorate for support and the hospitality which they extend to the non DESY members of the collaboration.

References

[1] C. Adloff *et al.* (H1 Collaboration), Z. Phys. **C 72** (1996), 593; C. Adloff *et al.* [H1-Collaboration], Nucl. Phys. **B 545** (1999) 21; A. Aktas *et al.* [H1-Collaboration], Eur. Phys. J. **C 51** (2007), 271.

[2] E. Laenen *et al.*, Phys. Lett. **B 291** (1992), 325.

[3] E. Laenen *et al.*, Nucl. Phys. **B 392** (1993), 162, ibid. 229; S. Riemersma, J. Smith, and W.L. van Neerven, Phys. Lett. **B 347** (1995), 143.

[4] B. W. Harris and J. Smith, Phys. Rev. **D 57** (1998), 2806 [hep-ph/9706334]; id. Nucl. Phys. **B 452** (1995), 109 [hep-ph/9503484]; id. Phys. Lett. **B 353** (1995), 535 [err. ibid **B359** (1995), 423] [hep-ph/9502312].

[5] M.A.G. Aivazis *et al.* , Phys. Rev. **D 50** (1994), 3102.

[6] J.C. Collins, Phys. Rev. **D 58** (1998), 094002.

[7] V. Gribov, L. Lipatov, Sov. J. Phys. **15** (1972), 438, ibid. 675; L. Lipatov, Sov. J. Phys. **20** (1975), 94; G. Altarelli, G. Parisi, Nucl. Phys. **B 126** (1977), 298; Y. Dokshitser, Sov. J. Phys. **46** (1977), 641.

[8] V.G. Kartvelishvili, A.K. Likhoded and V.A. Petrov, Phys. Lett. **B 78** (1978), 615.

[9] H1-collaborarion, *Study of Charm Fragmentation into $D^{*\pm}$-Mesons in Deep Inelastic Scattering at HERA*, contribution # 863, this conference.

[10] H. Jung, Comput. Phys. Commun. **86** (1995) 147; RAPGAP 3.2 program manual unpublished, http://www-h1.desy.de/∼jung/RAPGAP.html.

[11] H. Jung, Proc. 7th DIS Workshop, Nucl. Phys. (Proc. Suppl.) **B 79** (1999), 429.

[12] H. Jung, Proc. Workshop on Monte Carlo Generators for HERA Physics, 1998-1999, DESY-PROC-1999-02, p.75 [hep-ph/9908497]; H. Jung and G. Salam, Euro. Phys. J. **C 19** (2001), 351 [hep-ph/0012143].

[13] GEANT 3, R. Brun *et al.*, CERN-DD/EE/84-1.

[14] M. Ciafaloni, Nucl. Phys. **B 296** (1988), 49; S. Catani, F. Fiorani and G. Marchesini, Phys. Lett. **B 234** (1990), 339; S. Catani, F. Fiorani and G. Marchesini, Nucl. Phys. **B 336** (1990), 18; G. Marchesini, Nucl. Phys. **B 445** (1995), 49 [hep-ph/9412327].

[15] H. Jung, *Procs. of the XII International Workshop on Deep Inelastic Scattering (DIS 2004)*, Strbske Pleso, Slovakia, April 14-18, 2004, Eds. D. Bruncko, J. Ferencei and P. Strizenec, IEP SAS, Kosice, Vol. I, p.299 [hep-ph/0411287].

[16] I. Abt *et al.* [H1 Collaboration], Nucl. Instrum. Meth. **A 386** (1997), 310; ibid. 348.

[17] B. Andrieu *et al.* [H1 Calorimeter Group], Nucl. Instrum. Meth. **A 336** (1993), 460.

[18] B. Andrieu *et al.* [H1 Calorimeter Group], Nucl. Instrum. Meth. **A 336** (1993), 499; ibid. **A 344** (1994), 492; ibid. **A 350** (1994), 57.

[19] R. D. Appuhn *et al.* [H1 SpaCal Group], Nucl. Instrum. Meth. **A 386** (1997), 397.

[20] U. Bassler, G. Bernardi, Nucl. Instrum. Methods **A 361** (1995), 197 [hep-ex/9412004]; ibid. **A 426** (1999), 583 [hep-ex/9801017].

[21] P. Granet it et al. [French-Soviet-collaboration], Nucl. Phys. **B 140** (1978), 389.

[22] A. Jung on behalf of H1-collaboration, *D^*Production in DIS and Photoproduction at H1*, Proc. 16th Int. Workshop on Deep-Inelastic Scattering, April 2008, University College, London, UK, to be published; see also contribution # 855 this conference.

[23] A. Kwiatkowski, H. Spiesberger, and H.J. Möhring, Z. Phys. **C 50** (1991), 165.

[24] M.-O. Bönig, *Messung des D^*-Meson-Produktionsquerschnitts in tiefinelastischer Streuung mit dem H1-Experiment*, PhD Thesis, University of Dortmund, 2007.

[25] J. Pumplin *et al.*, JHEP **07** (2002), 012 [hep-ph/020195].

[26] W.K. Tung *et al.*, JHEP **0702** (2007), 053 [archiv:hep-ph/0611254].

[27] A.D. Martin, W.J. Stirling, and R.S. Thorne, Phys. Lett. **B 636** (2006), 259 [archiv:hep-ph/0603143].

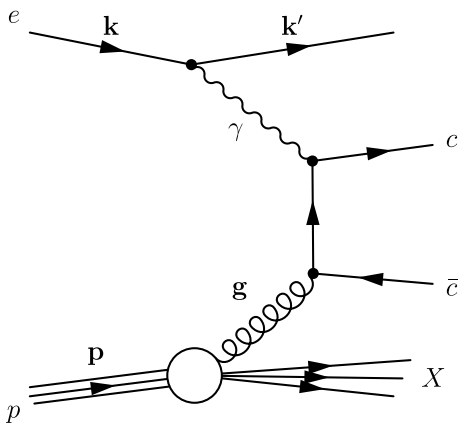

Figure 1: Leading order diagram of the boson-gluon fusion.

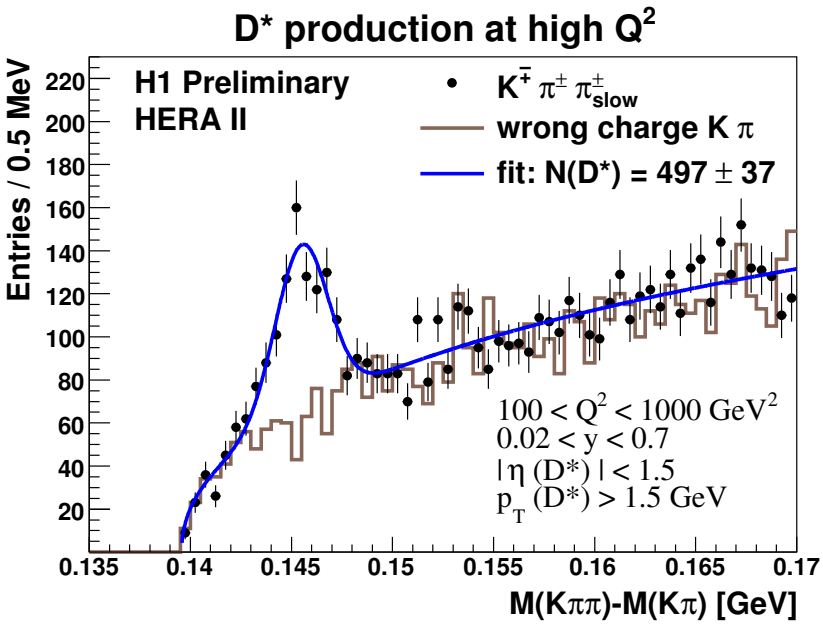

Figure 2: Δm distributions for all D^* candidates (data points). The histogram shows wrong charge combinations resembling the combinatorial background. The curve represents the result of the fit to the sum of signal and background (see text).

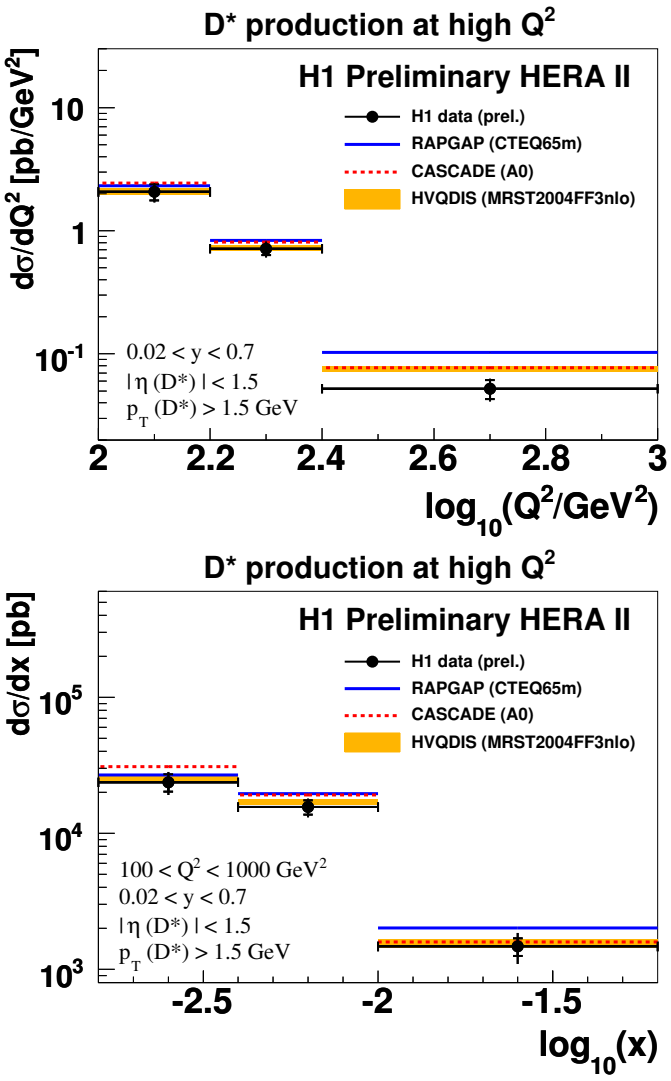

Figure 3: Differential cross sections as a function of $\log(Q^2)$ and $\log(x)$ compared with the predictions of the RAPGAP and CASCADE Monte Carlo simulations and the NLO calculation HVQDIS.

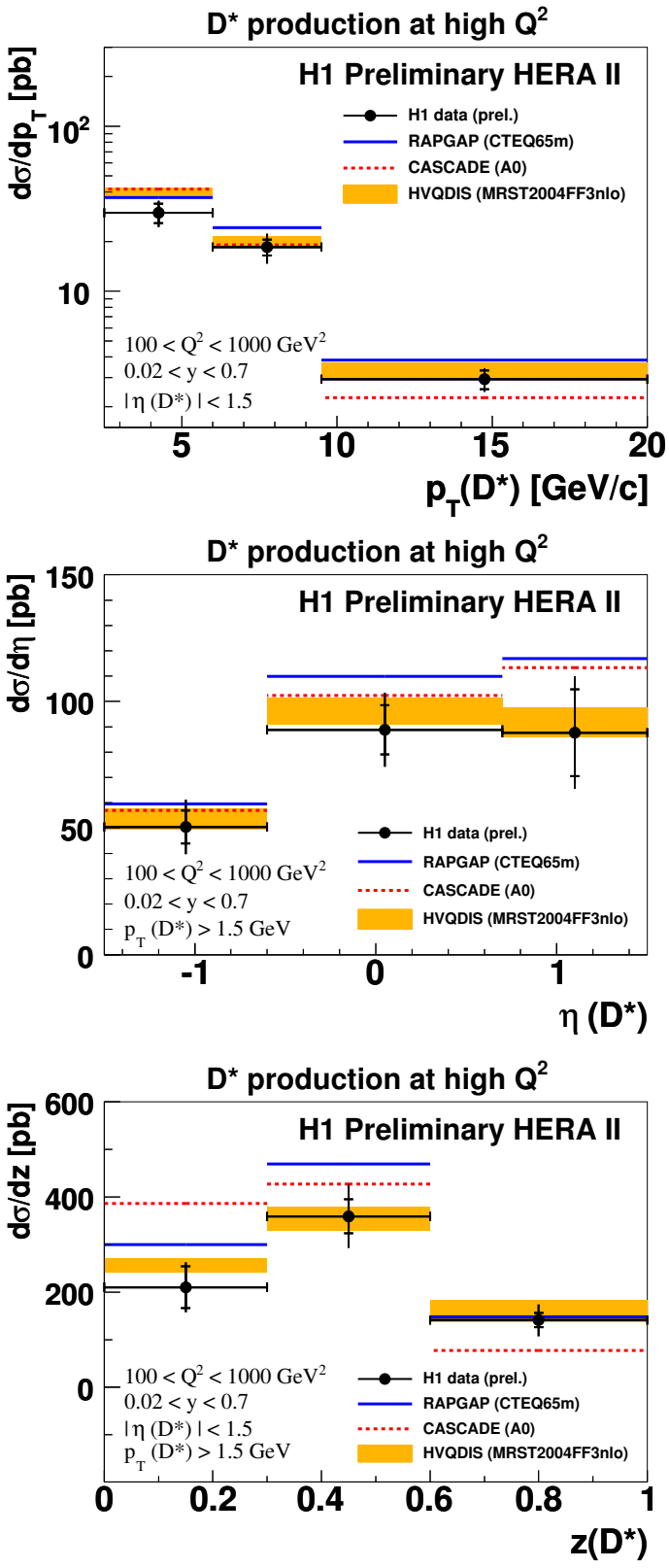

Figure 4: Differential cross sections as a function of $p_t(D^*)$, $\eta(D^*)$ and $z(D^*)$ compared with the predictions of the RAPGAP and CASCADE Monte Carlo simulations and the NLO calculation HVQDIS.

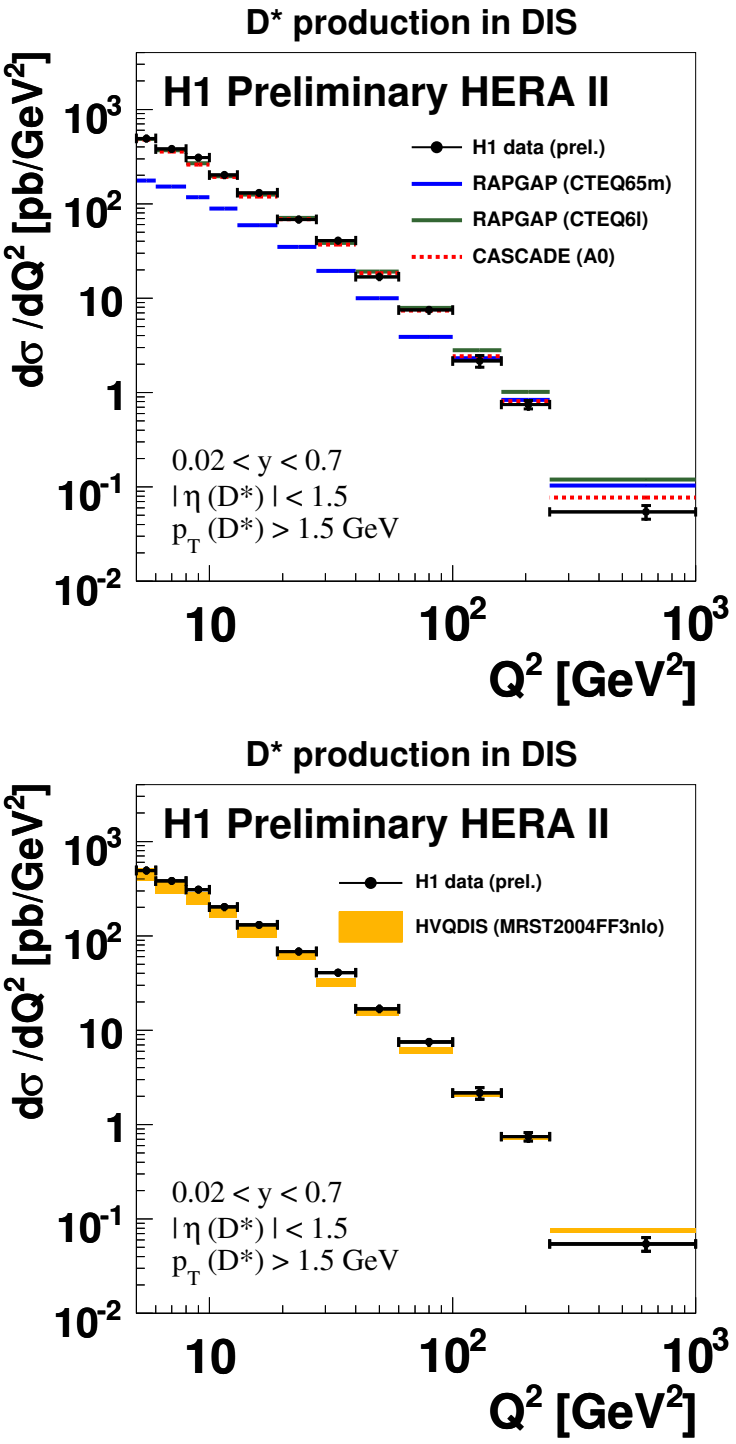

Figure 5: Differential cross sections as a function of Q^2 combined with the results of the medium Q^2 analysis [22]. In the upper plot the cross section is compared with the predictions of the RAPGAP and CASCADE Monte Carlo simulations, in the lower plot with the NLO calculation HVQDIS.